Arsenic(III) and Arsenic(V) Reactions with Zerovalent Iron Corrosion Products

ARTICLE *in* ENVIRONMENTAL SCIENCE AND TECHNOLOGY · JANUARY 2003

Impact Factor: 5.33 · DOI: 10.1021/es0206846 · Source: PubMed

4 AUTHORS, INCLUDING:

Bruce Manning
San Francisco State University, San Francisc…
23 PUBLICATIONS **3,256** CITATIONS

SEE PROFILE

Jory A Yarmoff
University of California, Riverside
178 PUBLICATIONS **4,338** CITATIONS

SEE PROFILE

Environ. Sci. Technol. **2002**, *36,* 5455−5461

Arsenic(III) and Arsenic(V) Reactions with Zerovalent Iron Corrosion Products

BRUCE A. MANNING,*,† MATHEW L. HUNT,‡ CHRISTOPHER AMRHEIN,‡ AND JORY A. YARMOFF§

Department of Chemistry and Biochemistry, San Francisco State University, 1600 Holloway Avenue, San Francisco, California 94132, Department of Environmental Sciences, University of California, Riverside, California 92521, and Department of Physics, University of California, Riverside, California 92521

Zerovalent iron (Fe^0) has tremendous potential as a remediation material for removal of arsenic from groundwater and drinking water. This study investigates the speciation of arsenate (As(V)) and arsenite (As(III)) after reaction with two Fe^0 materials, their iron oxide corrosion products, and several model iron oxides. A variety of analytical techniques were used to study the reaction products including HPLC-hydride generation atomic absorption spectrometry, X-ray diffraction, scanning electron microscopy-energy-dispersive X-ray analysis, and X-ray absorption spectroscopy. The products of corrosion of Fe^0 include lepidocrocite (γ-FeOOH), magnetite (Fe_3O_4), and/or maghemite (γ-Fe_2O_3), all of which indicate Fe(II) oxidation as an intermediate step in the Fe^0 corrosion process. The in-situ Fe^0 corrosion reaction caused a high As(III) and As(V) uptake with both Fe^0 materials studied. Under aerobic conditions, the Fe^0 corrosion reaction did not cause As(V) reduction to As(III) but did cause As(III) oxidation to As(V). Oxidation of As(III) was also caused by maghemite and hematite minerals indicating that the formation of certain iron oxides during Fe^0 corrosion favors the As(V) species. Water reduction and the release of OH^- to solution on the surface of corroding Fe^0 may also promote As(III) oxidation. Analysis of As(III) and As(V) adsorption complexes in the Fe^0 corrosion products and synthetic iron oxides by extended X-ray absorption fine structure spectroscopy (EXAFS) gave predominant As−Fe interatomic distances of 3.30−3.36 Å. This was attributed to inner-sphere, bidentate As(III) and As(V) complexes. The results of this study suggest that Fe^0 can be used as a versatile and economical sorbent for in-situ treatment of groundwater containing As(III) and As(V).

Introduction

Elevated levels of arsenic (As) in the environment are attributable to both natural and anthropogenic sources, including geologic parent materials, geothermal discharges, industrial products and wastes, agricultural pesticides, wood preservatives, and mine drainage (*1*−*7*). Drinking water that contains high As concentrations is a significant, well-recognized problem in many regions including the Bengal Delta (Bangladesh and West Bengal, India) (*5, 8*), the Red River Delta (Vietnam) (*9*), and many other areas including the western United States (*1*). Arsenic has been ranked as a high priority top 20 hazardous substance by the Agency for Toxic Substances and Disease Registry (ATSDR) (*10*) and is of particular concern due to chronic toxicity at relatively low concentrations (<100 ppb) that can be found in drinking water. Regulations put forward by the U.S. Environmental Protection Agency (USEPA) (*11*) to lower the As drinking water standard from 50 to 10 μg/L will require the development of simple, low cost methods for removal of As from drinking water.

The predominant forms of As in groundwater and surface water are the inorganic species arsenate [As(V)] and arsenite [As(III)]. The As(V) species exists as oxyanions ($H_2AsO_4^-$ and $HAsO_4^{2-}$) at neutral pH, whereas the As(III) species remains protonated as $H_3AsO_3^0$ at pH below 9.2 (*12, 13*). The mobility of As in soil and groundwater is closely dependent on redox environment and is most soluble under reducing conditions where As(III) predominates (*1, 12*−*14*). The close association between iron oxides and As has been demonstrated where both As(III) and As(V) are adsorbed on iron oxides forming inner-sphere surface complexes (*15*−*19*).

Many methods have been used to remove As from drinking water including anion exchange, precipitation, ion flotation, and adsorption (*20*−*26*). Attention has recently focused on zerovalent iron (Fe^0) as a reactive material for immobilizing As (*27*−*29*). Zerovalent iron has been extensively applied to remediation of contaminants such as chlorinated organic chemicals (*30*) and Cr(VI) (*31, 32*) in groundwater and has several advantages for As remediation. The primary advantages for application of Fe^0 to As remediation include low cost, simplicity in handling and scalability, and the formation of strong adsorption complexes between iron oxide reaction products and dissolved As(III) and As(V).

The oxidation of the Fe^0 surface is a spontaneous corrosion reaction that forms Fe(II) and Fe(III) and can act as an electron donor causing reduction of dissolved ions (*33*). Inorganic contaminants which are electrochemically reduced during Fe^0 corrosion include Cr(VI) (*31, 32*) and U(VI) (*34*). A recent study by Farrell et al. (*28*) has shown that dissolved As(V) does not participate in the electrochemical oxidation reaction of Fe^0. Rather, water molecules are the primary oxidant of the Fe^0 surface (water reduction) and that Fe(II) is the initial oxidation product:

$$Fe^0 + 2H_2O \rightarrow Fe^{2+} + H_2 + 2OH^- \qquad (1)$$

The Fe(II) formed at the corroding Fe^0 surface reacts with OH^- to form ferrous hydroxide ($Fe(OH)_2$) followed by oxidation to an Fe(II)/Fe(III) mixed phase such as magnetite over the course hours to days (*28, 35, 36*). This time-dependent process results in a gradient going from magnetite near the Fe^0 surface to maghemite (*28*).

Several recent investigations have shown that Fe^0 corrosion produces an efficient iron oxide sorbent for both As(III) and As(V) (*27*−*29*). The mechanism of As(III) and As(V) removal involves adsorption of As(III) and As(V) on iron oxide formed *in-situ* as a result of the Fe^0 corrosion reaction (*27*−*29*). The speciation of As after reaction with Fe^0 has been previously investigated and evidence for reduction of As(V) to As(III) remains mixed. Using XPS, Su and Puls (*29*) found

* Corresponding author phone: (415)338-1292; fax: (415)338-2384; e-mail: bmanning@sfsu.edu.
† San Francisco State University.
‡ Department of Environmental Sciences, University of California.
§ Department of Physics, University of California.

10.1021/es0206846 CCC: $22.00
Published on Web 11/07/2002

reduction of As(V) to As(III) on Fe^0 (Peerless Fe^0) where a steady distribution of 73−76% As(V) and 22−25% As(III) was achieved over 30−60 days in the solid-phase corrosion products. Lackovic et al. (*27*) found no evidence of As(V) reduction or As(III) oxidation in leachates from As(V)- and As(III)-treated Fe^0:sand column experiments over shorter time periods. Using a combination of X-ray absorption spectroscopy and HPLC analyses Farrell et al. (*28*) showed evidence of the formation of covalent, inner-sphere As(V) complexes on Fe^0 corrosion products and no evidence for As(V) reduction (*28*).

Based on the importance of determining the mechanism of removal of both As(III) and As(V) from drinking water, and outstanding questions about the As(III)/(V) speciation after reaction with Fe^0, the objectives of this study are as follows: (i) to determine the composition and identity of the iron oxide in the Fe^0 corrosion products; (ii) analyze the As(III)/(V) speciation in As(III)- and As(V)-treated Fe^0 and iron oxide model compounds using an advanced method (HPLC-hydride generation atomic absorption spectroscopy); and 3. perform a solid phase study of As(III)- and As(V)-treated Fe^0 and iron oxide model compounds using several techniques.

Materials and Methods

In all experiments, reagent grade $NaAsO_2$ (Mallinckrodt) and $Na_2HAsO_4 \cdot 7H_2O$ (Fisher) and deionized (DI) water were used to make As(III) and As(V) stock solutions. Background electrolyte used for experiments were prepared from either NaCl (Fisher) or HCl (Fisher trace metal). In certain experiments, tap water from Riverside, CA was used as a background medium. The two Fe^0 materials used in this study were a 100-mesh electrolytic Fe^0 powder (>99% total Fe, Fisher) used with no acid-washing (hereafter referred to as Fe^0-100) and 40-mesh degreased iron filings (Fe^0-40) that were fractionated by sieving (35−60 mesh sieve size). The fractionated Fe^0-40 filings were acid treated with 1% HCl for 1 h, rinsed with deionized water, and dried on a hot plate under N_2 gas.

Solid-Phase Analysis of Fe^0 Corrosion Products. Two corrosion materials (Rust-100 and Rust-40) were produced by reacting 4 g of the Fe^0-100 or Fe^0-40 in 1 L of 10.0 mM NaCl in a paddle-stirred reactor under aerated conditions for 4 days. The reactors were sonicated for 3 min at 10% power once a day. After magnetic separation of unreacted Fe^0 the rust products were filtered on 0.45 μm membranes and dried at 100 °C followed by X-ray diffraction (XRD) analysis with a Siemens D500 diffractometer using Cu Kα radiation. DIFFRAC-AT software was used to collect and analyze the XRD patterns. Sample peak positions were matched to known peak positions of standard minerals (*37*). Unreacted Fe^0, Rust-100, Rust-40, and As(V)-reacted Fe^0 samples were analyzed by scanning electron microscopy-energy-dispersive X-ray analysis (SEM-EDX) with an Amray 3200 (Amray Inc. Bedford, MA) under vacuum at 250−350 mTorr. SEM-EDX analysis was performed on samples reacted 24 h in 4 L plastic beakers with either zero or 0.027 mM As(V) in 1.0 mM NaCl and without stirring. Before SEM analysis the solids were rinsed with DI water and dried at 70 °C for 1 h.

Iron Oxide Minerals. Goethite (α-FeOOH) was made by a method outlined by Atkinson et al. (*38*). Lepidocrocite (γ-FeOOH) and maghemite (γ-Fe_2O_3) were synthesized by methods described by Schwertmann and Cornell (*36*). Hematite (α-Fe_2O_3) was made by heating magnetite to 750 °C for 6 h. The magnetite used in this study was of natural origin and originally contained some hematite coatings. The magnetite was citrate-dithionite (CD) treated until XRD peaks for hematite were relatively minor. After the CD reaction, the magnetite was rinsed with DI water, and oven dried at 105 °C. All iron oxides showed the dominant XRD peaks of their respective standards, except for maghemite which was poorly crystalline due to the method of synthesis (*36*). With the exception of magnetite before CD treatment, no impurities were observed in the XRD traces of the other oxides. Specific surface area was determined for all materials (Fe^0 and iron oxides) by Brunauer−Emmett−Teller (BET) N_2 adsorption.

Batch Reactions and Phosphate Extraction of As-Treated Fe^0. Batch reactions with Fe^0-100 and Fe^0-40 were carried out in 50 mL polycarbonate centrifuge tubes using a suspension density of 1.000 ± 0.009 g of Fe^0 in 25 mL of 0.20 or 2.0 mM As(III) or As(V) solution. The reactions were carried out at room temperature (23 ± 1 °C) and all treatments were duplicated. Tubes were shaken for 7.5 d (150 oscillations min^{-1}), followed by centrifugation (10000 rpm for 10 min), and filtration (0.45 μm) of the supernate. Treatments were designed to determine the effects of As(III) and As(V) concentration, pH, and gas atmosphere on the adsorption and speciation of As(V) on Fe^0-100 and Fe^0-40. The solids were then extracted with 25 mL of 10 mM PO_4 solution (NaH_2PO_4 and Na_2HPO_4, pH 7) by vortexing, shaking for 2 h, and solid/solution separation. Another experiment was conducted with both types of Fe^0, both rust products, and the iron oxide minerals. The reactions were carried out in 0.20 mM As(III) starting at pH 5 but without pH control. After 24 h the solutions were separated from the solids by centrifugation, filtration (0.45 μm), and PO_4 extraction of the solids (as above). In all batch experiments speciation for As(III) and As(V) in solutions and extracts was performed using high-performance liquid chromatography (HPLC) coupled with hydride generation-atomic absorption spectrophotometry (HGAAS) (*39*). (Tables summarizing the materials studied, surface area measurements, and qualitative results of batch reactions are provided as Supporting Information.)

X-ray Absorption Spectroscopy (XAS). Samples were prepared (as described above, but without PO_4 extraction) by treating Fe^0 and iron oxide with 2 mM As(III) or As(V) for EXAFS and X-ray absorption near-edge structure (XANES) analyses. The solids were rinsed with DI water to remove unreacted As and mounted on Teflon holders without drying. Standards included both solid and dissolved $NaAsO_2$ and $Na_2HAsO_4 \cdot 7H_2O$ and an As metal foil. All samples were analyzed at the Stanford Synchrotron Radiation Laboratory (SSRL) on beamline 7−3 with a 14−15 K liquid helium cryostat. A Si(220) double crystal monochromator with a 1 mm upstream aperture was used and was detuned 30% or more to reduce second-order harmonics. The K edge of As was scanned in a stepped mode in increments of 10 eV (between 11635 and 11845 eV), in 0.35 eV between 11845 and 11985 eV (XANES region), and 2 eV increments from 11985 to 12040 eV. X-ray fluorescence was collected with a 13-element Ge-detector (Canberra). An X-ray filter of Ge with a thickness of 6 absorption lengths was used to reduce scattered radiation from elements with atomic numbers less than As. Soller slits were used to reduce the fluorescent radiation from the filter. In addition, 3 to 6 sheets of aluminum foil were used to reduce the fluorescence from Fe relative to As.

The XAS spectra were analyzed using EXAFSPAK software (*40*). Individual X-ray scans were averaged together and background-corrected with a first order polynomial fit to the data 50 eV below the absorption edge. XANES data were normalized to the absorption edge or jump height (*41*). The K-edge inflection point was determined by measuring the eV at the maximum in the first derivative of the normalized spectra. The spectra were then normalized to unity using a Victoreen polynomial function. A spline function was fit to the "absorption envelope" and subtracted from the spectra over the energy range 11920 to 12869 eV. This isolated

TABLE 1. Speciation of As(III) and As(V) in Solution and Phosphate Extracts of As(III)-Treated Fe^0, Rust-100 and Rust-40 Corrosion Products, and Iron Oxides

	solution			sorbed As_T	PO_4 extract		as recovery
material	(t = 0 h) $[As(III)]_0$ (%)	(t = 24 h) [As(III)] (%)	(t = 24 h) [As(V)] (%)	(t = 24 h) [As(III+V)] (%)	(t = 26 h) [As(III)] (%)	(t = 26 h) [As(V)] (%)	(t = 26 h) [As(III+V)] (%)
Fe^0-100	100[a]	ND[b]	11.7	88.3	ND	2.64	14.3
Fe^0-40	100	0.05	0.20	99.8	0.05	1.39	1.69
rust-100	100	37.1	0.76	62.2	5.49	6.13	49.5
rust-40	100	1.74	0.03	98.2	9.20	1.38	12.4
goethite	100	0.27	ND	99.7	53.9	ND	54.1
lepidocrocite	100	1.95	0.19	97.9	13.9	ND	16.1
maghemite	100	0.18	ND	99.8	1.63	ND	1.81
magnetite	100	100	ND				100
hematite	100	100	ND				100

[a] At t = 0, $[As(III)]_0$ = 0.20 mM, 1.000 ± 0.009 g solid in 25 mL. [b] ND = not detected.

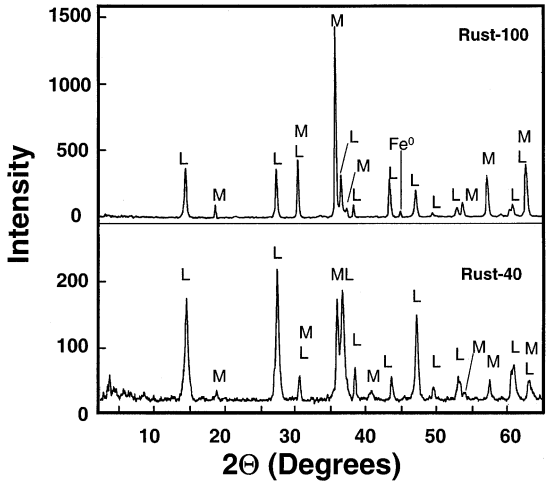

FIGURE 1. X-ray diffraction analysis of the iron oxide corrosion products formed from Fe^0-100 (Rust-100) and Fe^0-40 (Rust-40). Major peaks are due to lepidocrocite (γ-FeOOH) (L) and magnetite/maghemite (Fe_3O_4/γ-Fe_2O_3) (M).

function was then transformed from units of eV to $Å^{-1}$ to produce the EXAFS function ($\chi(k)$) where k ($Å^{-1}$) is the photoelectron wave vector. The $\chi(k)$ function was weighted by k^3 and a truncated k-range (k-window) of 2.00 to 12.5 $Å^{-1}$ was used for further analysis.

The k^3-weighted $\chi(k)$ function ($\chi(k)\times k^3$) was then Fourier transformed (FT) and the radial structure function (RSF) in R-space (Å) was created. The two major peaks in the RSF (As−O and As−Fe shells) were isolated by selecting the R-window as the minimum amplitude points at low and high distance points around the peaks resulting in As−O and As−Fe R-windows. The individual As−O and As−Fe R-windows, and the composite As−O + As−Fe R-window (1.02−3.30 Å), were back-transformed to produce the Fourier filtered (FF) EXAFS functions. In all cases, the unfiltered, raw EXAFS spectra were used in the final parameter fitting process.

Experimental EXAFS data were fit with coordination number (N), interatomic distance (R), and the Debeye−Waller parameter (σ^2). An additional variable, the energy offset (E_0), was a fitted parameter in the filtered As−O shell data, and held constant for all subsequent fits. Phase and amplitude functions for the absorber and backscatterers were defined using the single scattering, curved wave FEFF model (*42, 43*). Error estimates for the parameters fitted to unfiltered data were R ± 0.09 Å, N ± 20%, and σ^2 ± 20−30%.

Results

Solid-Phase Analysis of Fe^0 Corrosion Products. Analysis of Rust-100 and Rust-40 by XRD indicates the presence of lepidocrocite and magnetite and/or maghemite (Figure 1). Rust-100 gave higher XRD peak intensities and evidence of more crystalline iron oxides than Rust-40. Because magnetite and maghemite are isostructural, and were effectively indistinguishable by our XRD data, either oxide may be present. These phases, in addition to akaganeite (β-FeOOH) and goethite (α-FeOOH), were also found by Gu et al. (*44*) in Fe^0 corrosion products from column studies. The strong XRD peaks at 14.1 and 27.1 degrees 2θ (6.26 and 3.29 Å, respectively) were in agreement with reference standard lepidocrocite crystallographic d-spacings (*37*). Both lepidocrocite and magnetite form from oxidation of Fe(II) (*35*).

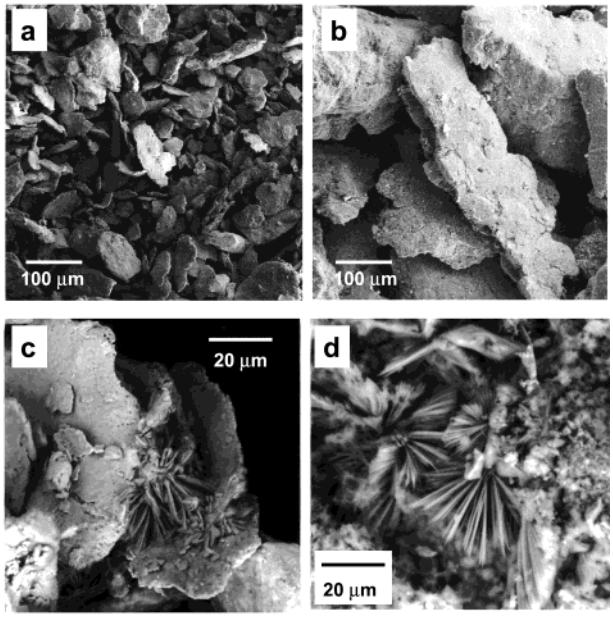

FIGURE 2. SEM images of (a) unreacted Fe^0-100, (b) unreacted Fe^0-40, (c) corroded Fe^0-100, and (d) corroded Fe^0-40. Both Fe^0 materials were reacted 24 h in 0.027 mM As(V) in 1.0 mM NaCl.

The SEM image of unreacted Fe^0-100 by SEM (Figure 2a) reveals a platelike morphology with relatively smooth surfaces and particle sizes ranging from 10 to 100 μm in diameter. The unreacted Fe^0-40 particles are subangular grains with much narrower particle size distribution ranging from 200 to 400 μm in diameter and 500−1000 μm in length (Figure 2b). Though the Fe^0-100 had much smaller particle size, the Fe^0-40 particles appeared to have a rougher surface. This may account for the higher BET surface area on Fe^0-40 (3.50 $m^2\ g^{-1}$) than the Fe^0-100 (0.10 $m^2\ g^{-1}$) material (see Table 1 Supporting Information). The Fe^0-40 had a higher As(III) and As(V) adsorption capacity than Fe^0-100 on a gram weight

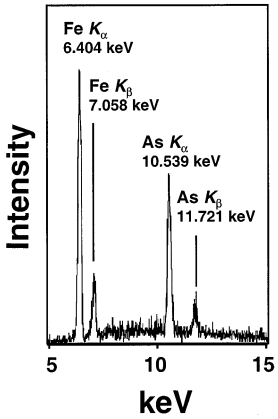

FIGURE 3. Energy-dispersive X-ray analysis of As(V)-treated Fe^0-40 24 h in 0.027 mM As(V) in 1.0 mM NaCl.

basis suggesting that Fe^0-40 particle surfaces were more readily corroded to iron oxides. The SEM images of Fe^0-100 and Fe^0-40 reacted with As(V) (Figure 2, parts c and d, respectively) display laths or plates of iron oxide corrosion product approximately 20 μm in length emanating from central corrosion loci. The relatively smooth surfaces of the Fe^0-100 surfaces are evident (Figure 2c), whereas Fe^0-40 surfaces show a more advanced layer of corrosion (Figure 2d). The lath/plate crystal morphology is attributed to lepidocrocite (*35*). The XRD data in Figure 1 and the lath features suggest the primary crystalline iron oxide component of the Rust-40 is lepidicrosite.

The EDX spectrum of As(V)-treated Fe^0-40 (Figure 3) gives the characteristic X-ray emission peaks for Fe K_α, Fe K_β, As K_α, and As K_β at 6.404, 7.058, 10.54, and 11.72 keV, respectively (*45*). The EDX method is not purely a surface technique because X-rays are generated from a region of approximately 2 μm in depth by the electron beam. However, this is representative of the reacted surface region. Though the EDX method used here is not quantitative, the intensity of the As K_α and As K_β emission relative to Fe K_α and Fe K_β suggests a high As(V) loading (>0.1% As in the EDX spot volume) in the film of corrosion product. We estimate the mixed iron oxide corrosion product incorporates As(V) into the solid to loadings as high as 15% w:w.

Batch As(V)-Fe^0 and As(III)-Fe^0 Reaction Studies. The potential for As(V) reduction to As(III) by direct electrochemical coupling with Fe^0 oxidation was investigated by As(III)/(V) speciation using HPLC−HGAAS. (A table of treatments and results of these experiments are provided as Supporting Information.) The 0.20 and 2.0 mM As(V) treatments both resulted in 100% As(V) uptake during Fe^0 corrosion yielding As loadings of 5.0 and 50 mmol g^{-1} Fe^0, respectively. Treatments with tap water (initial pH 7.8) and 1.0 mM HCl (initial pH 3.2) had pH values of >9.0 and ~7.5, respectively after 7.5 d of equilibration. Regardless of Fe^0 material, solution matrix, or gas atmospheric control, no evidence for As(V) reduction to As(III) by electrochemical coupling with Fe^0 corrosion was found after the 7.5 d period.

Reduction of inorganic ions such as CrO_4^{2-} (*31*), SO_4^{2-} (*44*), and UO_2^{2+} (*34*) by Fe^0 has been reported, though previous work on $HAsO_4^{2-}$ has found no evidence for As(V) reduction to As(III) or As(0) (*27*, *28*, *46*). An XPS investigation by Su and Puls (*29*) also found no evidence of short-term (5 d) reduction of As(V) by Fe^0, though long-term (60 d) reduction of As(V) to As(III) on Fe^0 was evident. Recent work by Melitas et al. (*46*) has concluded that the electrochemical potential required to reduce As(V) to As(III) is lower than the potential produced at the corroding Fe^0 surface in aqueous solution.

The reaction of As(III) with Fe^0 was investigated using similar batch adsorption conditions as As(V), and the results

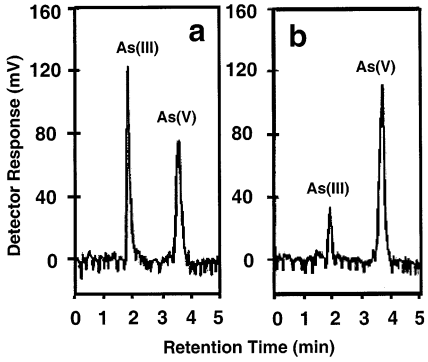

FIGURE 4. HPLC−HGAAS chromatograms showing (a) 0.13 μM As(III) + 0.13 μM As(V) and (b) the PO_4 extract of As(III)-treated Fe^0-40.

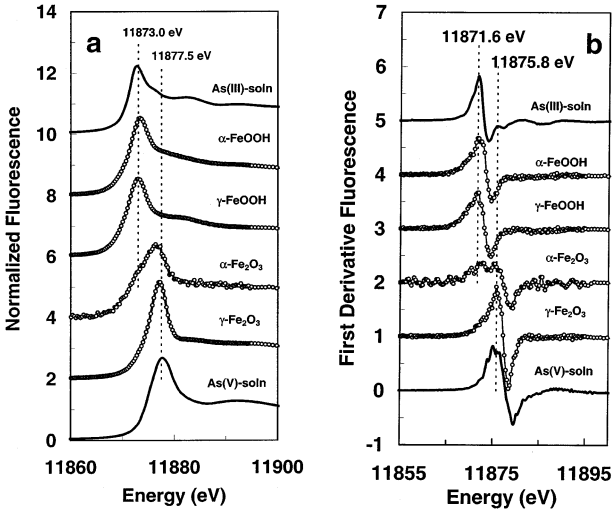

FIGURE 5. X-ray absorption data showing (a) XANES edges and (b) first derivative plots of As(III)/(V) standard solutions and As(III)-treated iron oxides.

are given in Table 1. Greater than 97% of As(III) was adsorbed by Fe^0-40, Rust-40, goethite, lepidocrocite, and maghemite, whereas no detectable As(III) adsorption was observed on magnetite or hematite over the 24 h time period. Detectable As(III) adsorption on magnetite and hematite was found only after longer time periods (>2 d). The Fe^0-100 and Rust-100 adsorbed 88.3 and 62.2% As(III), respectively. The difference between the adsorption capacities of Fe^0-40 and Fe^0-100 may be due to differences in the initial Fe^0 surface area. A higher surface area would increase the surface corrosion rate on Fe^0 and show a greater surface adsorption reactivity. Measurable As(V) in the As(III)-treated Fe^0-100 initial reaction solution was 11.7% and As(III) was not detectable (Table 1).

Extraction of the As(III)-treated Fe^0-40, Rust-40, and Rust-100 with PO_4 yielded mixtures of As(III) and As(V) (Table 1). Only As(V) was extracted from As(III)-treated Fe^0-100. Figure 4 shows representative HPLC−HGAAS chromatograms of an equimolar (0.13 μM) As(III):As(V) mixed standard (Figure 4a) and a diluted PO_4 extract of As(III)-treated Fe^0-40 (Figure 4b). The recovery of As(V) in the PO_4 extract of As(III)-treated Fe^0-40 was greater than that of Rust-40 (Table 1) suggesting that the in-situ corrosion reaction was an important factor in causing As(III) oxidation. Arsenic(V) was not detected in the reaction solutions or PO_4 extracts of As(III)-treated goethite, lepidocrocite, or maghemite.

As(III) and As(V) XANES Analyses. A complete set of XANES data are shown for the As(III)-treated samples in Figure 5. The As(III) and As(V) standard solutions are shown as references, and the absorption maxima occur at 11873 and 11877.5 eV, respectively. Oxidation of As(III) causes a

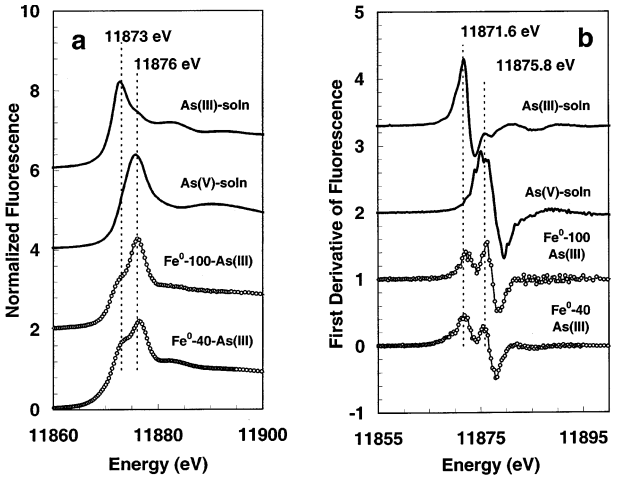

FIGURE 6. XANES edges and first derivative plots of As(III)/(V) standard solutions and As(III)-treated Fe^0 materials.

shift in the X-ray absorption edge to a higher energy (approximately 2 eV per unit oxidation state change). Analysis of the XANES first derivative curves for the As(III)-treated materials resulted in an X-ray absorption edge shift of 4.2 eV when As(III) and As(V) are compared (Figure 5b). The As(V)-treated samples will be discussed in more detail in the discussion of EXAFS (below).

Goethite and lepidocrocite showed substantial As(III) adsorption but did not oxidize As(III) (Figure 5a). Hematite and magnetite sorbed As(III) only weakly (up to 40 mg kg^{-1} As) under the XANES experimental conditions and gave poor quality XANES spectra. Nonetheless, the As(III)-treated hematite spectrum is included as an example of a mixed As(III)/As(V) system. A mixed As(III)/As(V) system results in a shoulder in the X-ray absorption edge and two peaks in the first derivative curve. Maghemite showed both strong As(III) adsorption (Table 1) and oxidation properties as exhibited by a single maximum peak in the first derivative plot in line with the As(V) standard (Figure 5b).

The XANES analyses of As(III)-treated Fe^0 gave clear evidence of partial As(III) oxidation to form a mixed As(III)/As(V) speciation in the solids (Figure 6a,b). The energy of the two first derivative peaks for As(III)-treated Fe^0-100 and Fe^0-40 corresponded closely to the energy values for the As(III) and As(V) standards. There was no evidence found for As(III) oxidation by the X-ray beam. Though the XANES technique is not a quantitative measurement, the data are qualitatively in agreement with the PO_4 extraction data (Table 1).

Understanding the mechanism of As(III) oxidation on the corroding Fe^0 surface is complicated by many factors including such questions as whether As(III) is oxidized during the Fe^0 corrosion reaction process or after and hence involving one of the Fe^0 corrosion products. Oxidation of As(III) by Fe^0 may also be the result of mineral impurities such as Mn oxides (*29*). A previous study (*47*) found that iron oxides and oxyhydroxides synthesized from Fe(II) were capable of rapid As(III) oxidation. Formation of an electrochemical potential gradient on the corroded Fe^0 particle results in passivating films of magnetite and maghemite which are likely formed from Fe(II) (*28*). Another intriguing factor is the pH-dependence of the As(III) oxidation reaction according to previous work which has shown that As(III) auto-oxidizes at pH greater than the first pK_a for As(III) (pH = 9.2) (*48*). Postreaction pH values in the present study were typically >9.0 and thus it is likely that As(III) was exposed to a high pH environment. Locally elevated pH is the result of water reduction on the surface of corroding Fe^0 (eq 1) resulting in the release of OH^- to solution near the surface of corroding Fe^0 (*28*, *49*).

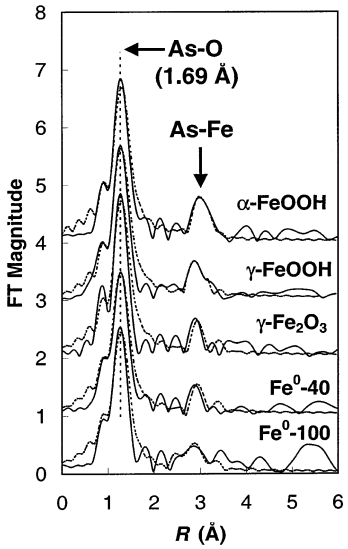

FIGURE 7. Radial structure functions from EXAFS analysis of As(V)-treated iron oxides and Fe^0 materials. Solid lines are experimental data and dotted lines are the theoretical fits.

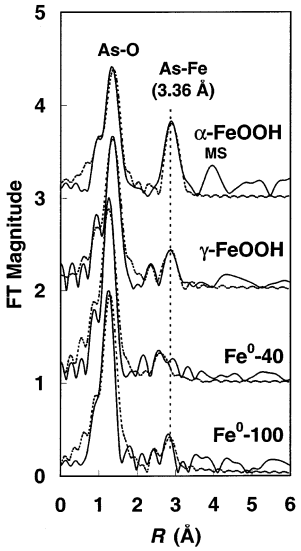

FIGURE 8. Radial structure functions from EXAFS analysis of As(III)-treated iron oxides (goethite and lepidocrocite) and Fe^0 materials. Solid lines are experimental data and dotted lines are the theoretical fits. The multiple scattering (MS) shell on goethite was not included in the fit.

The experimental radial structure functions (RSF) produced from Fourier transformed EXAFS data are shown in Figures 7 and 8 (solid lines). These data were not phase corrected. The fits of the theoretical EXAFS expression to the experimental data are also shown (dotted lines, Figures 7 and 8), and the fitted parameters are given in Tables 2 (As(V)-treatment) and 3 (As(III)-treatment). The magnetite and hematite samples were not further analyzed by EXAFS due to poor signal:noise ratios. The predominant feature in Figure 7 is a coherent shell of 4.0−4.2 oxygen atoms at an As−O interatomic distance of 1.69 Å. This distance corresponds closely to previous EXAFS studies (*18*, *28*) and is diagnostic for the As(V) species. The As(V)-treated iron oxides/oxyhydroxide samples in Figure 7 were successfully described by two As−Fe shells (Table 2). The second shell in the Fourier transform plots are the result of As−Fe correlations composed of approximately 2.00 Fe atoms ($As-Fe_1$) at 3.36 ± 0.06 Å, 3.34 ± 0.06 Å, and 3.38 ± 0.06 Å for goethite, lepidocrocite, and maghemite, respectively. Considering the error estimate

TABLE 2. EXAFS Fit Parameter Results for As(V)-Treated Iron Oxides and Zerovalent Iron

sample	interatomic shell	N^a	R (Å)	σ^2 (Å^{-1})
α-FeOOH	As−O[b]	4.00	1.70	0.00060
	As−Fe_1	2.00	3.36	0.00050
	As−Fe_2	1.00	3.53	0.01954
γ-FeOOH	As−O	4.00	1.69	0.00060
	As−Fe_1	2.01	3.34	0.00370
	As−Fe_2	1.00	3.50	0.00644
γ-Fe_2O_3	As−O	4.00	1.69	0.00050
	As−Fe_1	2.18	3.38	0.00306
	As−Fe_2	1.15	3.54	0.00152
Fe(0)−40	As−O	4.00	1.69	0.00090
	As−Fe_1	2.30	3.37	0.00400
	As−Fe_2	1.10	3.51	0.00200
Fe(0)−100	As−O	4.00	1.69	0.00100
	As−Fe_1	1.30	3.05	0.00400
	As−Fe_2	2.10	3.36	0.00800

[a] N = coordination number, R = interatomic distance, σ^2 = Debye−Waller parameter. [b] Fits were achieved by analyzing Fourier filtered As−O and As−Fe shells independently, followed by fitting the composite As−O + As−Fe spectra. Only one As-backscatterer shell was allowed to vary at a time.

TABLE 3. EXAFS Fit Parameter Results for As(III)-Treated Iron Oxides and Zerovalent Iron

sample	interatomic shell	N^a	R	σ^2
α-FeOOH	As−O[b]	3.10	1.78	0.00240
	As−Fe_1	2.00	3.34	0.00105
	As−Fe_2	1.00	3.46	0.00106
γ-FeOOH	As−O	3.30	1.79	0.00180
	As−Fe_1	1.00	3.09	0.00231
	As−Fe_2	2.00	3.39	0.01818
Fe(0)−40	As−O	3.90	1.71	0.00220
	As−Fe_1	1.00	3.00	0.00300
	As−Fe_2	2.00	3.30	0.02100
Fe(0)−100	As−O	3.60	1.70	0.00180
	As−Fe_1	1.00	3.08	0.00175
	As−Fe_2	2.00	3.39	0.07000

[a] N = coordination number, R = interatomic distance, σ^2 = Debye−Waller parameter. [b] Fits were achieved by analyzing Fourier filtered As−O and As−Fe shells independently, followed by fitting the composite As−O + As−Fe spectra. Only one As-backscatterer shell was allowed to vary at a time.

of ±0.06 Å, these distances are similar to an As−Fe shell of 3.30 Å previously reported for As(V)-treated goethite (*15*, *18*). This distance has been ascribed to a bidentate, binuclear As(V) surface complex where the AsO_4 tetrahedron is attached to adjacent apexes of edge-sharing Fe octahedra. An additional As−Fe shell of approximately 1.00 Fe atom at 3.52 ± 0.06 Å (As−Fe_2) resulted in improvements in the EXAFS fit and may be the result of a mononuclear As(V)-Fe surface complex (*15*, *17*).

The As(V)-treated Fe^0 samples were also analyzed by EXAFS (Figure 7). The As−O shells were well described by 4.00 O atoms at an average distance of 1.69 Å. Arsenic(V) reduction would result in a shift of the As−O shell from 1.69 to 1.78 Å accompanied by a decrease in As−O peak amplitude but no such effects were detectable. The Fe^0-40 sample displayed EXAFS and Fourier transform data which were similar to the maghemite (γ-Fe_2O_3) sample, including the As−Fe_1 and As−Fe_2 shells. This suggests that maghemite may be an important sorbent phase in the Fe^0-40 corrosion product. The As(V)-treated Fe^0-100 sample suffered from signal:noise degradation as indicated by the large peak in the FT plot between 5 and 6 Å (Figure 7). A shell of 1.30 Fe atoms at 3.05 Å plus a more pronounced contribution from a shell of 2.10 Fe atoms at 3.36 Å gave a reasonable fit to the data. The As−Fe_1 shell at 3.05 Å may be the result of bidentate, mononuclear shared edge complex with a single Fe octahedron (*15*).

Examination of the As−O shells in the RSF data shown in Figure 8 and Table 3 suggest that As(III) was oxidized to As(V) during corrosion of Fe^0-40 and Fe^0-100 but was not oxidized by goethite or lepidocrocite. The As(III) adsorption complexes on goethite and lepidocrocite were described by 3.10 and 3.30 O atoms at As−O interatomic distances of 1.78 and 1.79 Å, respectively (Table 3). A third peak in the As(III)-goethite RSF was attributed to multiple scattering (MS) and was not included in the fit. The As−O shells in the As(III)-treated oxyhydroxides have longer interatomic distances and a smaller amplitude than the As(III)-treated Fe^0 samples (Figure 8) which is a clear indication of As(V) formation.

Implications for Drinking Water Remediation. We have presented evidence that As(III) is oxidized to As(V) during the Fe^0 corrosion reaction under aerobic conditions. This reaction is advantageous due to the conversion of As(III) to a less toxic As(V) and the formation of strongly adsorbed and coprecipitated As(V) on iron oxide products. The reaction products after corrosion of Fe^0 are a heterogeneous mixture of the iron oxides lepidocrocite and either magnetite or maghemite in both the Fe^0-40 and Fe^0-100 materials. Oxidation of As(III) was caused by the in-situ Fe^0 corrosion reaction as well as certain synthetic iron oxides (hematite and maghemite). The use of Fe^0 to remove both As(III) and As(V) from water has promising potential, and engineering studies to develop this technology are ongoing. The results of this study underscore the importance of Fe^0 as both a robust and economical material for the in-situ treatment of contaminants. The formation of the iron oxide sorbent and the potential to oxidize As(III) to As(V) makes Fe^0 a particularly good candidate for treatment of water with elevated levels of As.

Acknowledgments

This research was supported in part by the U.S. Department of Agriculture National Research Initiative Competitive Grants Program (Project 9604171), a DuPont Educational Aid Program Grant, and the U.S. Department of Energy Environmental Management Science Program (Project DE-FG07-96ER14707).

Supporting Information Available

Chemical formulas, origin, and surface area of zerovalent iron and iron oxide materials and treatments and qualitative results for zerovalent iron materials reacted with As(III) and As(V). This material is available free of charge via the Internet at http://pubs.acs.org.

Literature Cited

(1) Welch, A. H.; Lico, M. S.; Hughes, J. L. *Ground Water* **1988**, *26*, 333−347.
(2) Nicolli, H. B.; Suriano, M. A.; Peral, G.; Ferpozzi, L. H.; Baleani, O. A. *Environ. Geol. Water Sci.* **1989**, *14*, 3−16.
(3) Sadler, R.; Olszowy, H.; Shaw, G.; Biltoft, R.; Connell, D. *Water, Air, Soil Pollut.* **1994**, *78*, 189−198.
(4) Ong, C. G.; Herbel, M. J.; Dahlgren, R. A.; Tanji, K. K. *Environ. Sci. Technol.* **1997**, *31*, 831−836.
(5) Chakraborti, D.; Samanta, G.; Mandal, B. K.; T. R. Chowdhury, T. R.; Chanda, C. R.; Biswas, B. K.; Dhar, R. K.; Basu, G. K.; Saha, K. C. *Curr. Sci.* **1998**, *4*, 346−355.
(6) Rösner, U. *Environ. Geol.* **1998**, *33*, 224−230.
(7) Wilkie, J. A.; Hering, J. G. *Environ. Sci. Technol.* **1998**, *32*, 657−662.
(8) Lepkowski, W. *Chem. Eng. News* **1998**, *76*, 27−29.
(9) Berg, M.; Tran, H. C.; Nguyen, T. C.; Pham, H. V.; Schertenleib, R.; Giger, W. *Environ. Sci. Technol.* **2001**, *35*, 2621−2626.

(10) Agency for Toxic Substances and Disease Registry. Top 20 Hazardous Substances: ATSDR/EPA Priority List for 1997. http://atsdr1.atsdr.cdc.gov: 8080/cxcx3.html.
(11) *Fed. Regist.* **2001**, *66*(14), 6975−6976.
(12) Korte, N. E.; Fernando, Q. *Crit. Rev. Environ. Control* **1991**, *21*, 1−39.
(13) Masscheleyn, P. H.; Delaune, R. D.; Patrick, W. H., Jr. *J. Environ. Qual.* **1991**, *20*, 522−527.
(14) Masscheleyn, P. H.; Delaune, R. D.; Patrick, W. H., Jr. *Environ. Sci. Technol.* **1991**, *25*, 1414−1419.
(15) Waychunas, G. A.; Rea, B. A.; Fuller, C. C.; Davis, J. A *Geochim. Cosmochim. Acta* **1993**, *57*, 2251−2269.
(16) Manceau, A. *Geochim. Cosmochim. Acta* **1995**, *59*, 2251−2269.
(17) Fendorf, S. E.; Eick, M. J.; Grossl, P.; Sparks, D. L. *Environ. Sci. Technol.* **1997**, *31*, 315−320.
(18) Foster, A. L.; Brown, G. E., Jr.; Tingle, T. N.; Parks, G. A. *Am. Mineral.* **1998**, *83*, 553−568.
(19) Manning, B. A.; Fendorf, S. E.; Goldberg, S. *Environ. Sci. Technol.* **1998**, *32*, 2383−2388.
(20) Zouboulis, A. I.; Kydros, K. A.; Matis, K. A. *Sep. Sci. Technol.* **1993**, *28*, 2449−2463.
(21) Zhao, Y.; Zouboulis, A. I.; Matis, K. A. *Sep. Sci. Technol.* **1996**, *31*, 769−785.
(22) Waypa, J. J.; Elimelech, M.; Hering, J. G. *J. Am. Water Works Assoc.* **1997**, *89*, 102−114.
(23) Cheng, R. C.; Liang, S.; Wang, H.-C.; Beuhler, M. D. *J. Am. Water Works Assoc.* **1994**, *86*, 79−90.
(24) Harper, T. R.; Kingham, N. W. *Water. Environ. Res.* **1992**, *64*, 200−203.
(25) Hering, J. G.; Chen, P.-Y.; Wilkie, J. A.; Elimelech, M. *J. Environ. Eng.* **1997**, *123*, 800−807.
(26) Edwards, M. *J. Am. Water Works Assoc.* **1994**, *86*, 64−78.
(27) Lackovic, J.; Nikolaidis, N. P.; Dobbs, G. M. *Environ. Eng. Sci.* **2000**, *17*, 29−39.
(28) Farrell, J.; Wang, J.; O'Day, P.; Conklin, M. *Environ. Sci. Technol.* **2001**, *35*, 2026−2032.
(29) Su, C.; Puls, R. W. *Environ. Sci. Technol.* **2001**, *35*, 1487−1492.
(30) Johnson, T. J.; Scherer, M. M.; Tratnyek, P. G. *Environ. Sci. Technol.* **1996**, *30*, 2634−2640.
(31) Pratt, A. R.; Blowes, D. W.; Ptacek, C. J. *Environ. Sci. Technol.* **1997**, *31*, 2492−2498.
(32) Blowes, D. W.; Ptacek, C. J.; Jambor, J. L. *Environ. Sci. Technol.* **1997**, *31*, 3348−3357.
(33) Cantrell, K. J.; Kaplan, D. I.; Weitsma, T. W. *J. Hazard. Mater.* **1995**, *42*, 201−212.
(34) Gu, B.; Liang, L.; Dickey, M. J.; Yin, X.; Dai, S. *Environ. Sci. Technol.* **1998**, *32*, 3336−3373.
(35) Schwertmann, U.; Taylor, R. M. In *Minerals in Soil Environments, Second Edition*; Dixon, J. B.; Weed, S. B., Eds.; SSSA Book Series Number 1; Soil Science Society of America: Madison, WI, 1989; pp 379−438.
(36) Schwertmann, U.; Cornell, R. M. *Iron Oxides in the Laboratory*; VCH Publishers: New York, 1991; pp 6−12.
(37) Joint Committee on Powder Diffraction Standards (JCPDS). *Powder Diffraction File: Inorganic Phases.* International Centre for Diffraction Data: Swarthmore, PA, 1985.
(38) Atkinson, R. J.; Posner, A. M.; Quirk, J. P. *J. Phys. Chem.* **1967**, *71*, 550−558.
(39) Manning, B. A.; Martens, D. A. *Environ. Sci. Technol.* **1997**, *31*, 171−177.
(40) George, G. N.; Pickering, I. J. *EXAFSPAK: A Suite of Computer Programs for Analysis of X-ray Absorption Spectra;* Stanford Synchrotron Radiation Laboratory, Stanford, CA, 1993.
(41) Fendorf, S. E.; Sparks, D. L. In *Methods of Soil Analysis: Part 3-Chemical Methods*; Sparks, D. L., Page, A. L., Helmke, P. A., Loeppert, R. H., Soltanpour, P. N., Tabatabai, M. A., Johnson, C. T., Sumner, M. E., Eds.; SSSA Book Series Number 5; Soil Science Society of America: Madison, WI, 1996; pp 377−416.
(42) Rehr, J. J.; Mustre de Leon, J.; Zabinsky, S. I.; Albers, R. C. *J. Am. Chem. Soc.* **1991**, *113*, 5135−5140.
(43) Mustre de Leon, J.; Rehr, J. J.; Zabinsky, S. I.; Albers, R. C. *Phys. Rev. B* **1991**, *44*, 4146−4149.
(44) Gu, B.; Phelps, T. J.; Liang, L.; Dickey, M. J.; Roh, Y.; Kinsall, B. L.; Palumbo, A. V.; Jacobs, G. K. *Environ. Sci. Technol.* **1999**, *33*, 2170−2177.
(45) *Handbook of Chemistry and Physics*, 72nd ed.; Lide. D. R., Ed.; Chemical Rubber Publishing Company: Boca Raton, FL, 1991; pp 10−243 to 10−248.
(46) Melitas, N.; Conklin, M.; Farrell, J. *Environ. Sci. Technol.* **2002**, *36*, 3188−3193.
(47) De Vitre, R.; Belzile, N.; Tessier, A. *Limnol. Oceanogr.* **1991**, *36*, 1480−1485.
(48) Manning, B. A.; Goldberg, S. *Environ. Sci. Technol.* **1997**, *31*, 2005−2001.
(49) Uhlig, H. H.; Revie, R. W. *Corrosion and Corrosion Control*, 3rd ed.; John Wiley: New York, 1985.

Received for review April 9, 2002. Revised manuscript received September 19, 2002. Accepted September 25, 2002.

ES0206846